ADVANCED MATERIALS TECHNOLOGIES
www.advmattechnol.de

Wearable Perovskite Films for On-Line Monitoring of Radiotracers in Nuclear Medicine

Laura Basiricò, Matteo Verdi, Andrea Ciavatti,* Lorenzo Piergallini, Elisa Grassi, Federica Fioroni, Lorenzo Margotti, Nicolò Tosi, Valentina Cicero, Alessandro Montanari, Mauro Iori, and Beatrice Fraboni*

On-line in situ monitoring of radiation emitted by radiotracers during intravenous injection is of crucial importance for the safety of patients and personnel involved in nuclear medicine treatments and analysis. The aim of this work is to assess wearable perovskite ionizing radiation detectors for such application. With this purpose pixelated direct detector based on thin films of 2D layered perovskite PEA_2PbBr_4 are tested for the monitoring of gamma-rays emitted by ^{18}F radiopharmaceutical under different experimental conditions. The wearable detector is here demonstrated being able to detect in real-time the gamma-rays emitted by annihilation of ^{18}F radiotracer. Its reliability is assessed by ^{18}F half-life measurement with a maximum accuracy deviation within 8%. The detector also successes in its validation for the foreseen application, demonstrating able to monitor in real-time the whole injection process and extravasation event.

1. Introduction

The fighting against cancer is a worldwide compelling priority. Nuclear medicine represents one of the most important tools for early cancer diagnoses, therapeutic treatments and prognostic analysis, as testified by the forecasted growth of the market for novel therapeutic radioisotopes for cancer therapy by 2030.[1]

Despite the procedures for intravenous injection of radiopharmaceuticals are well established, extravasation events may occur when the administered radioactivity or part of it accumulates outside the venous system.[2] This happens due to improper injection procedures or a vessel's wall malfunction. Even partial extravasations may be critical, since they change the pharmacokinetics of the radiopharmaceutical used in diagnosis or in therapy and compromise, for example, the accuracy of PET (Positron Emission Tomography) imaging. PET is an imaging technology that uses radiopharmaceuticals, i.e., compounds labeled with positron emitting radionuclides, as molecular probes to image and in vivo measure biochemical processes.[3] After emission, each positron travels through the surrounding material and there is a continuous loss in its energy until it combines with an electron to either annihilate completely and emit a pair of 511 keV photons, or to form a very short-lived particle called positronium. The positronium is unstable, and within a fraction of a second, it decays into a pair of 511 keV photons. In both cases the emitted pair of 511 keV photons, i.e., the annihilation photons, are emitted in opposite directions at approximately 180° from each other. The radionuclide ^{18}F has become the major PET isotope for its physical properties (half time: 1.83 h, energy of beta emissions: 634 keV; percentage of beta emissions: 97%; energy of gamma emissions: 511 keV, percentage gamma emissions: 194%)[4] and for the worldwide use of 2-[fluorine-18]fluoro-2-deoxy-D-glucose (FDG), which has a crucial role in providing important tumor-related qualitative and quantitative metabolic information, that is critical to diagnosis and follow-up.[5] In particular, the Standardized Uptake Value (SUV) is a semiquantitative measure of normalized radioactivity concentration in PET images and its estimation may be affected by extravasation of ^{18}F labeled pharmaceuticals.[6] Besides diagnostics, in radionuclide therapy radiopharmaceuticals are intravenously administered to selectively treat tumors. The labeled compound represents the vector for the radionuclides, that emit particles, which deposit their energy in the surrounding tissues. These radioisotopes are mainly beta emitters, such as ^{177}Lu, which is largely used in peptide receptor radionuclide therapy and targeted radioligand therapy.[7]

L. Basiricò, M. Verdi, A. Ciavatti, L. Margotti, B. Fraboni
Department of Physics and Astronomy University of Bologna Viale Berti Pichat 6/2
Bologna40127, Italy
E-mail: laura.basirico2@unibo.it; andrea.ciavatti2@unibo.it

L. Basiricò, M. Verdi, A. Ciavatti, N. Tosi, V. Cicero, A. Montanari, B. Fraboni
National Institute for Nuclear Physics—INFN section of Bologna Viale Berti-Pichat 6/2
Bologna40127, Italy

L. Piergallini, E. Grassi, F. Fioroni, M. Iori
Medical Physics Unit
Azienda USL-IRCCS di Reggio Emilia
Reggio Emilia42123, Italy

The ORCID identification number(s) for the author(s) of this article can be found under https://doi.org/10.1002/admt.202401111

DOI: 10.1002/admt.202401111

In both cases (usage of radiopharmaceuticals for diagnoses[8] and for radionuclide therapies[9]), extravasations can cause severe damage of healthy tissues of the patient, e. g. epithelial rash or even necrosis. The damage is measured as absorbed dose, expressed in Gy, deposited by the particles emitted by the radionuclides. Wearable real-time detecting systems are thus of critical importance for safety both for patients (an early extravasation alert) and for personnel (supporting the wide-spreading of automatic injection machines).[10] Personal dosimeters currently available on the market and employed for real-time gamma-ray detection relies on scintillators (e.g., CsI (TI)) coupled with Si-PMT or Si-PD which, despite the high performances, are rigid, sometimes inaccurate in measurements, uncomfortable for the patient and not scalable on large areas with limited costs.[11] Further, as indirect detecting systems, they suffer from intrinsic lower spatial resolution with respect to the direct ones, i.e., a strong limitation in imaging applications.

In recent years lead halide perovskites have been assessed as high performing novel active materials for the direct detection of ionizing radiation in the form of single crystals,[12] wafers,[13] thick,[14] and thin[15] films.[16,17] If from one side, single crystals and thick layers assure the highest absorption of radiation thanks to the large volume of interaction, on the other side the employment of thin layers allows the fabrication of flexible devices, opening for wearable sensor application.[18] In addition, the limited interaction volume with radiation makes thin films more radiation tolerant, ensuring an extremely longer operational stability than thicker counterparts[19–21] and allowing for low bias or passive operation, a further key peculiarity for portability and wearability. These features are extremely appealing for in situ and online monitoring of the dose received by patients during therapies and diagnostic treatments with radiotracers. The possibility of designing lightweight wearable patches of conformable shapes and dedicated geometries (e.g., that can be wrapped around the arm during injection procedures), while maintaining the high sensitivity to ionizing radiation needed to detect the radioactive emission from the liquid solution injected in the body, would represent an important innovative tool toward patient's safety and treatment personalization. Although gamma-ray spectroscopy has been demonstrated by perovskite single crystals, showing excellent discrimination and performance,[22,23] the direct detection of high energy photons by perovskite thin film-based devices is instead very challenging due to their poor quantum efficiency. Recently, low dimensional hybrid organic/inorganic halide perovskites have attracted a great interest as active layer in direct ionizing radiation detection.[21,24,25] The key property that makes them appealing for high-energy photon detection is their intrinsic low dark current, due to lower intrinsic charge density than the 3D counterpart, ascribed to a lower self-doping in 2D perovskites. This effect has been reported by Peng et al.,[26] who proposed that crystallization of hybrid perovskites containing large organic cations (such as 2D perovskites) suppresses defect formation, favoring thus a low self-doping level. Additionally, the suppressed ion migration in 2D perovskites leads to higher stability of the dark current under continuously applied bias, further enhancing Signal to Noise Ratio (SNR) and Limit of Detection of high-energy radiation such as gamma-rays.

In this work we demonstrate how 2D perovskite thin film direct detectors can be employed for the online and real-time monitoring of radiation provided by gamma-ray emitting radiotracer commonly used in nuclear medicine. We provide the experimental proof of principle for extravasation event detection and for the effectiveness of an implemented wearable battery-operated system for such application.

2. Results and Discussion

^{18}F is a positron emitter with a half-life of 109.7 min[4] used as radiotracer in PET imaging systems. The emitted positron annihilates with a nearby electron emitting two 511 keV photons in opposite directions. **Figure 1a** schematizes the decay process of ^{18}F and the annihilation photons detected by the PET scanner. In this work, the ^{18}F radiotracer solution has been prepared as detailed in Experimental Section, with the final aim to validate thin-film perovskite-based detectors for the real-time monitoring of extravasation event occurring during radiopharmaceutical injection. PET images, collected at IRCCS Reggio Emilia, Italy (Discovery MI PET /CT scanner, GE Healthcare, Milwaukee, USA) and reported in Figure 1b,c (study approved by the Ethics Committee, Registration number 448/2021/SPER/IRCCSE), show the result of a safe injection and of an extravasation event, respectively, with the darker region in Figure 1c corresponding to the dangerous accumulation of radiotracer in the patient's arm.

The here reported perovskite-based detector is a 4-pixel matrix where each pixel has a 2-terminal photoconductor architecture, with a bottom interdigitated contact structure and the radiation impinging from the top of the active layer (see schematic in **Figure 2a**). In this kind of device, i.e., a photoconductive detector, the semiconductor is placed between two ohmic contacts, therefore by applying an external bias voltage, a measurable equilibrium current (dark current) flows in the device channel. Upon the exposure to ionizing radiation the carrier concentration in the active layer increases, producing an increment of the equilibrium current (photocurrent), proportionally to the energy released by the pulse of radiation.[27] In the here presented detector, the active layer is based on 2D layered perovskite, namely PEA_2PbBr_4 (PEA = $C_6H_5C_2H_4$), polycrystalline films directly deposited by spin-coating on a pixelated flexible substrate. The typical crystal structure of this material consists of sheets of $[PbBr_6]^{4-}$ octahedra, intercalated between bilayers of $C_6H_5C_2H_4NH_3^+$ organic spacers, as shown in the sketch reported in Figure 2a,b reports the linear attenuation coefficient of PEA_2PbBr_4: at 511 keV the linear coefficient results about 0.23 cm^{-1}, between the values of Cadmium Telluride (CdTe) and silicon (Si), i.e., two of the benchmark materials for direct gamma-ray detection.[28] The spin-coated film resulted in a polycrystalline layer with an average thickness of 1.9 ± 0.8 µm (over a batch of 20 samples fabricated with the same recipe), covering the whole matrix (Figure 2c). Such thickness range allows to combine film uniformity and good mechanical properties (see Figure S1, Supporting Information). Flexible plastic substrates (i.e., polyethylene terephthalate—PET—125 µm thick) were patterned with interdigitated Cr/Au electrodes using photolithography as detailed in Experimental Section. The resulting device exhibits high uniformity between the pixels, as testified by the overlapping current-voltage characteristics reported in Figure 2d (log–log plot reported in Figure S2, Supporting Information). The resulting average resistance value is (1.64 ± 0.14) × 10^{12} Ω. As

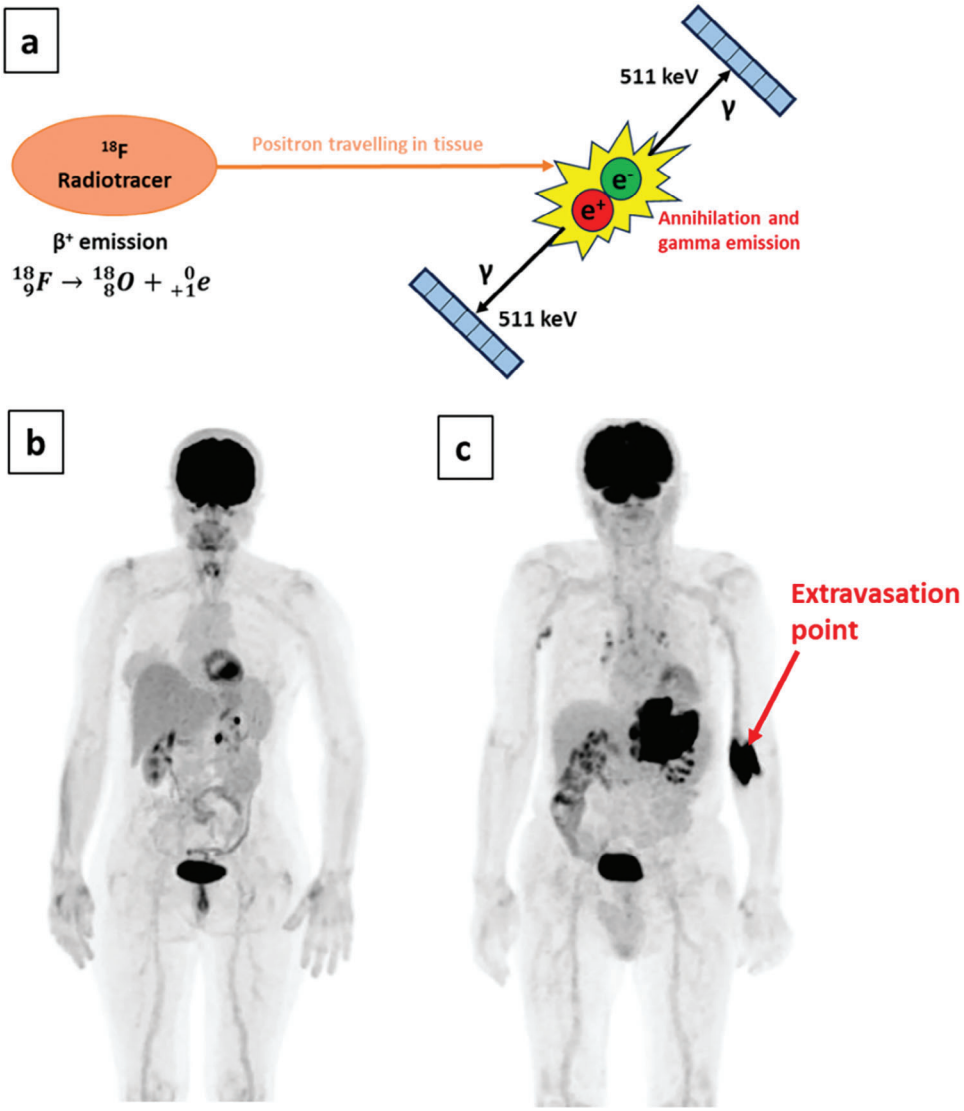

Figure 1. a) Schematic representation of radioactive decay of ^{18}F followed by the positron-electron annihilation and gamma-ray emission and detection. b) PET imaging of a safe administration of radiopharmaceutical. c) PET imaging of an extravasation event (indicated by the red arrow).

already mentioned in our previous work on similar devices characterized as direct X-ray detectors,[25] the dark current measured during this experiment is exceptionally low for a non-diode architecture, without the need of any interlayer in the device structure. This feature is crucial for the here targeted application since it assures high SNR value necessary to detect high-energy (511 keV) gamma rays emitted during ^{18}F emitted positron annihilation despite the moderate absorption due to the thin film structure.

To assess the capability of the detector to effectively detect gamma rays emitted by the radiotracer we developed a custom experimental setup shown in **Figure** 3a,b and Movie S1 (Supporting Information). This is equipped with a 3D-printed frame that holds in place a stepper motor and the sample box. The ^{18}F radioactive drug is contained into a vial kept by a printed support connected to the motor axis. A thick Pb cylinder is used to screen the sample from the radiation when the state is in the OFF position, while in the ON position the motor moves the gamma source on top of the sample. Further details are given in experimental section. Three radiotracer solutions with different activities between 1800 and 94 MBq were prepared and measured with a calibrated commercial detector (ISOMED 2000, Nuclear System). The shutter was set with a period of 20 s with duty cycle of 50%. Every three peaks the source was changed while the shutter was in the OFF state. The dynamic response is reported in Figure 3c. The device, biased at 2 V, shows a steep increase of the photocurrent in the ON state, followed by a decrease to the pristine dark current value in the OFF state. Although the first three peaks are not properly stable, the remaining peaks even at low activity are repeatable. We speculate that the instability measured at high activities can be attributed to a polarization effect, reported in literature for perovskite-based X-ray detectors under high fluxes.[29] The amplitude of the response well-scales with the activity, as evidenced in the plot of Figure 3d.

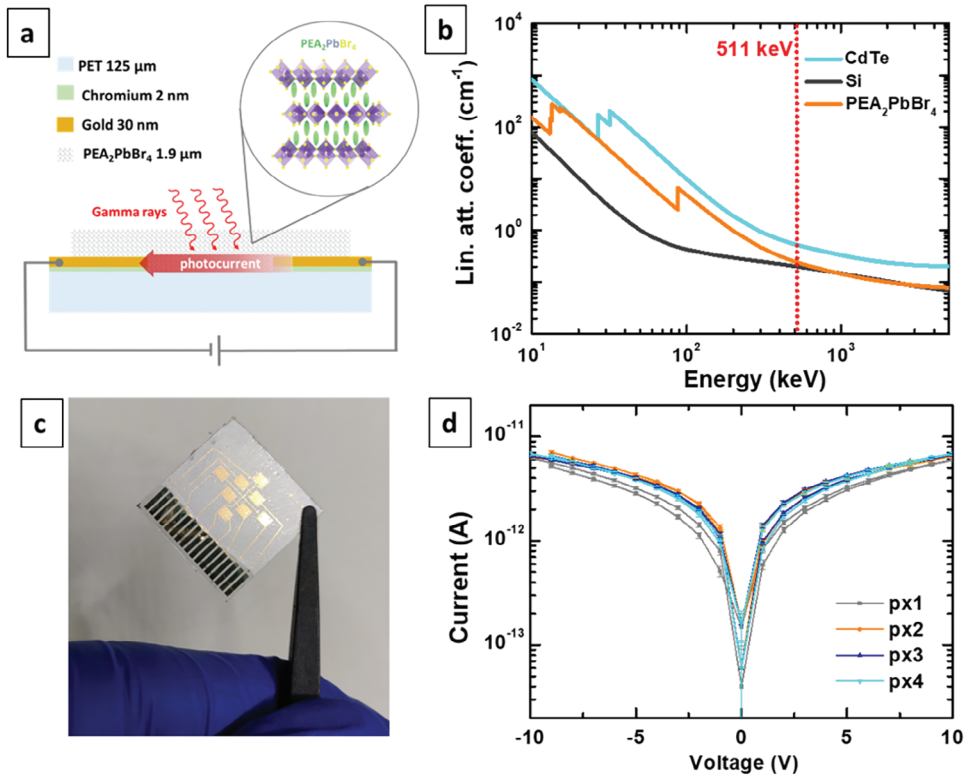

Figure 2. a) Schematic representation of the device structure and of the structure of PEA_2PbBr_4 perovskite composing the active layer of the here reported detector. b) Linear attenuation coefficient in function of photon energy of PEA_2PbBr_4 perovskite and two benchmark materials for gamma-ray detectors, i.e., Si and CdTe. The dashed orange line indicates the characteristic energy of gamma-ray emission due to positron annihilation following ^{18}F decay. c) Picture of the perovskite detector under study. d) Plot of the current versus voltage measurements of the 4 pixels. The error bars are calculated from the instrument's accuracy.

To further assess the reliability of the detector we followed the decay of ^{18}F with each of the 4 pixels. First, we verified that the photocurrent responses of the 4 pixels at the same irradiation conditions, i.e., exposed to ^{18}F at 328 MBq and biased at 5 V, i.e., a higher bias voltage with respect to that employed for the measurements reported in Figure 2c, to achieve a higher signal amplitude while keeping the dark current reasonably low and with as small drift. All the pixels properly and consistently responded to irradiation, as shown in the plot reported in **Figure** 4a.

Then, the device was positioned underneath the radiotracer vial and kept there for more than 4 h. To acquire the signal a portable, battery powered electronic board with Bluetooth was used. With this configuration, the source and the sample were kept in a closed room and the measurement was controlled safely. As reported in Figure 4b, the 4 pixels showed very similar response, with an exponential decay following the natural radioactive decay of fluorine, starting from an activity of 1.8 GBq.

The signal over time is described as $I\,(t) = I_{F18}\,(t) + I_{dark}$. I_{F18} is proportional to the number of detected events, thus, following the exponential law of radioactive decay, results:

$$I\ \ (t) = \ I_o e^{-\lambda \cdot t} + I_{dark} \tag{1}$$

where $I\,(t)$ is the current signal over time, I_o is the initial current at the beginning of acquisition, λ is the radioactive decay constant and I_{dark} is the dark current of the pixel. We plotted the data of Figure 4b as:

$$\ln\ \left(I - \ I_{dark}\right) = \ -\lambda\, t + \ \ln I_0 \tag{2}$$

^{18}F half-life values were estimated from fitting the experimental data of Equation (2), as reported in Figure S3 (Supporting Information). The average value over the four pixels is (108 ± 1) min, in accordance with the theoretical value, and with the maximum accuracy deviation within 8% (see Figure 4c).

To validate the detector for its actual application as radiation monitor for nuclear medicine treatments, we setup an experiment mimicking an extravasation event after the radiotracer injection procedure. **Figure** 5a shows the experimental configuration employed for this test. A phantom with plastic tubing was used to simulate the blood vessels in the patient's arm. The radioactive drug, with a blue dye added in the solution to make the flow easily visible, was injected in the phantom vein by a lead-shielded syringe. The activity used for the experiment was estimated based on assessments of the extravasation areas identified in the cohort of patients enrolled in the study approved by the Ethics Committee (Registration number 448/2021/SPER/IRCCSE). The main vein was simulated by an almost straight plastic tube, while the extravasation region, close to the detector, was simulated by a plastic tube rolled up. The experimental sequence is reported in Figure 5b and showed in Movie S2

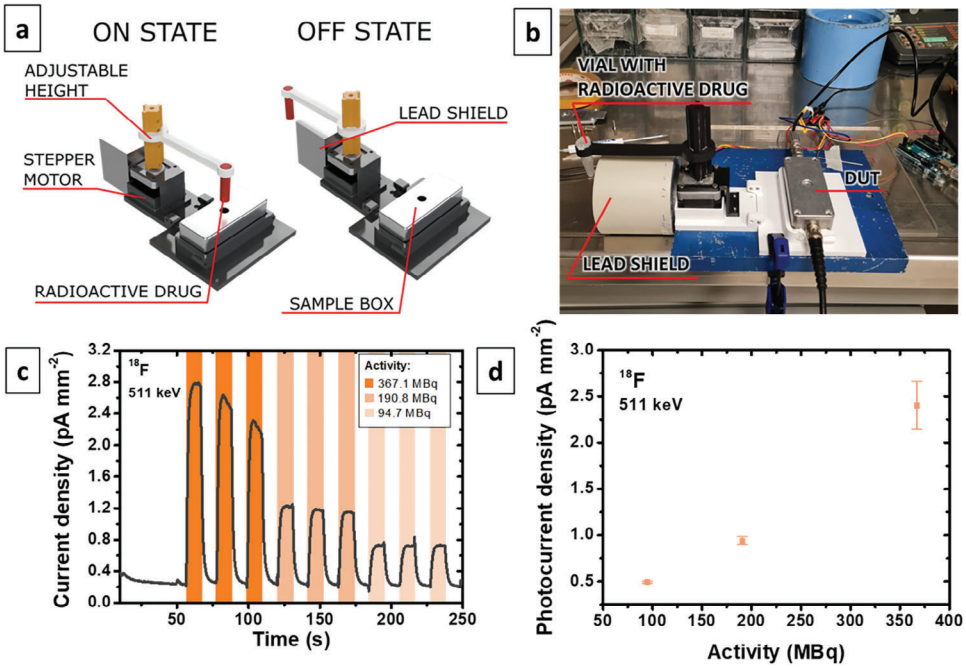

Figure 3. a) Schematics and picture (b) of the shutter system employed for the sensors characterization under high energy gamma ray emitted by radioactive drugs. A stepper motor is controlled by an Arduino UNO board. 3D printed holders keep the moto and sample box in place. The radioactive drug is contained in a vial hold by a custom support connected to the motor axis. c) Dynamic response at 2 V of PEA_2PbBr_4 detector. The data were collected using three ^{18}F with decreasing activity with a source to sample distance of 8 mm. d) Photocurrent density as a function of the source activity. Data has been calculated as the average of the three signals reported in c) collected for each activity value and the associated error bar as the standard deviation.

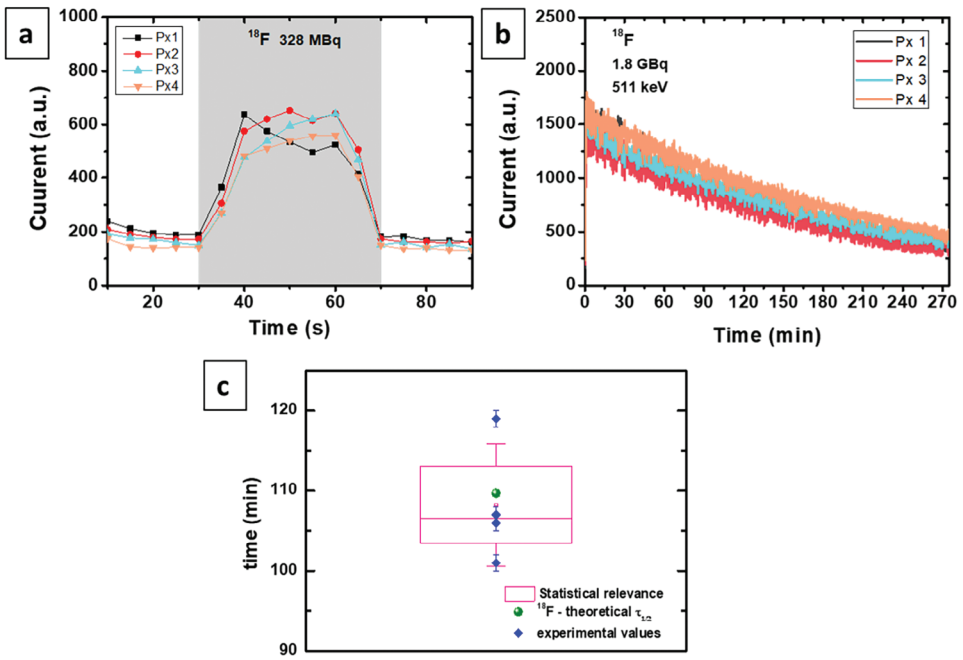

Figure 4. ^{18}F decay. a) Photocurrent signals of the 4 pixels biased at 5 V, exposed to ^{18}F at 328 MBq. b) Current signal from 4 different detector pixels positioned underneath a ^{18}F source for more than 4 h. c) ^{18}F half-life measurement.

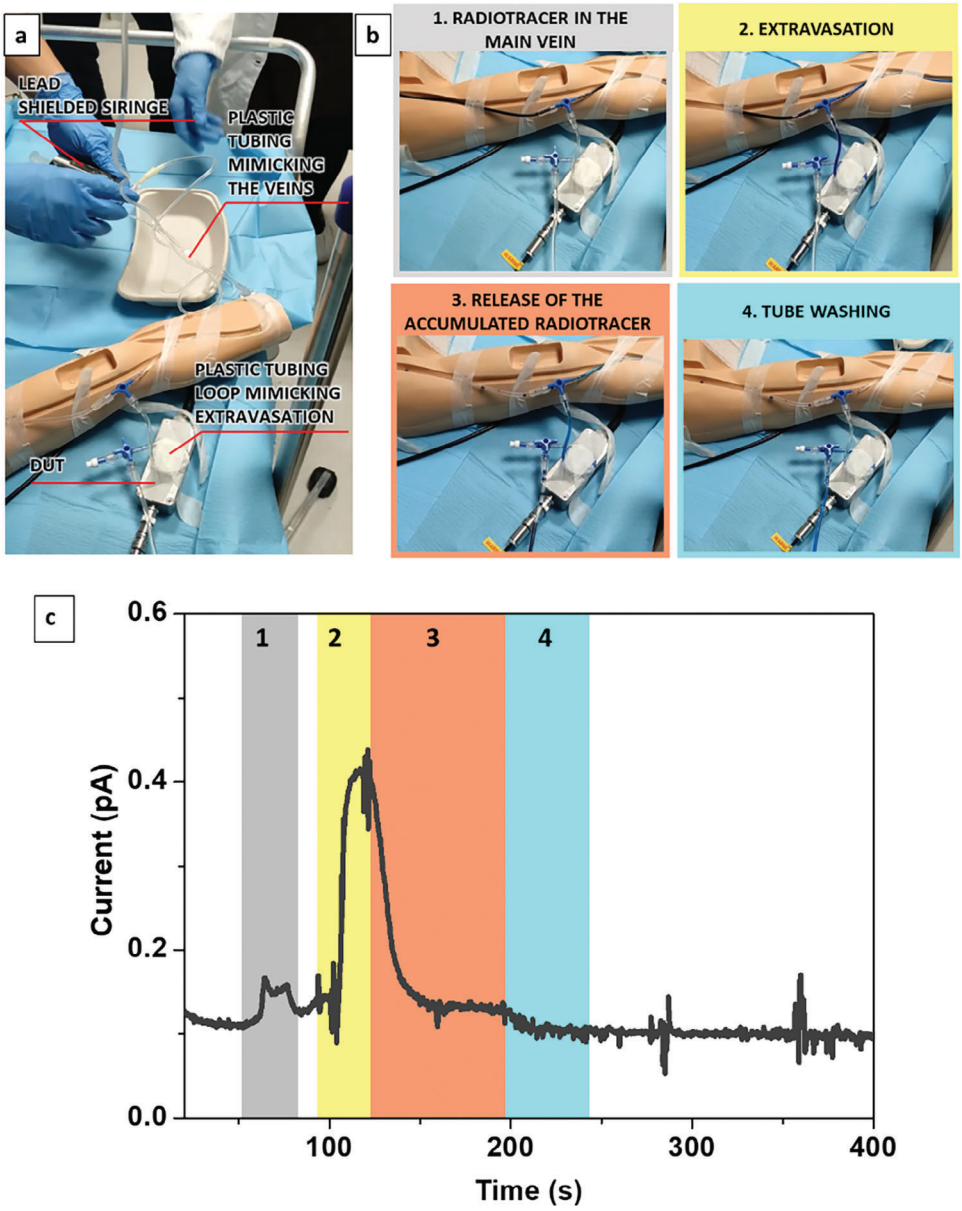

Figure 5. Monitoring radiotracer extravasation. a) Picture of the whole experimental setup used to mimic the extravasation event. b) Different steps in the injection procedures: 1. the blue colored radiotracer solution is injected in the plastic main tube simulating the vein. 2. The valve controlling the extravasation is opened and the radiotracer starts to flow in the secondary line rolled up and placed over the sample box simulating the accumulation of radiotracer in an unwanted region of the body. 3. After a while the extravasation line is opened, and the radiotracer starts to flow away from the detector (blue color is less intense). 4. Physiological solution is injected in the system flushing away the remaining radiotracer. c) Detector current signal, acquired at 2 V, during the whole injection procedure described above. The colored region refers to different test steps according to b).

(Supporting Information). Hereafter we list the sequence used to simulate the extravasation shown in Figure 5:

1) Injection (grey). The radiotracer is injected in the main vein, and it flows to the opposite direction of the injection point (toward the heart, in the real case). In the picture (Figure 5b), an intense blue color is visible.
2) Extravasation (yellow). A valve is opened causing a partial flow of radiotracer in the secondary tube accumulating above the detector.
3) Release of the accumulated radiotracer (orange). A valve at the end of the system is opened causing the radiotracer accumulated over the detector to flow away.
4) Flushing (cyano). At the end, physiological solution is released inside the tube cleaning all the system from the radioactive drug.

Figure 5c reports the recorded signal, the colored regions correspond to the different steps in the injection procedure. The detector reliably monitored the whole process. A small increase in

Figure 6. a) Wireless and wearable electronic readout system, connected to the detector through a flat cable. b) Detector system worn by the arm of an anthropomorphic phantom. c) Signal recorded and transmitted via WiFi, monitoring the gamma rays emitted by the flow of ^{18}F radiotracer inside the plastic tubing of the phantom mimicking the vein. The signal was collected with a detector bias voltage of 2 V.

the current was measured soon after the injection of the radiotracer in the main vein. When the valve was opened leading the extravasation, a higher increase in the sensor current was observed. The current started to decrease immediately when the accumulated radiotracer was released from the extravasation region. A low current signal remained until the physiological solution reached the extravasation region and cleaned the tube from the ^{18}F atoms. After few seconds the signal returned to the base line level. The detector demonstrates to be able of measuring the low amplitude of the signal emitted by a radiotracer, thanks to the unique dark current stability of 2D perovskite.

Finally, we tested a wearable system with custom readout electronics to provide the final proof of concept for real-time and online monitoring of radiotracer emissions. The compact battery-powered device is equipped with two adjustable laces (**Figure 6a**), through which it was mounted directly on the arm of the anthropomorphic phantom (Figure 6b). The sensors are connected through a short flat flexible cable that allows them to be placed exactly on the desired position. The onboard electronics can digitize the signal with a resolution of 0.2 pA at a 10 Hz sampling rate. The measured signals are transmitted via WiFi connection to a computer for data visualization and recording (Figure 6c). Even without the usage of high precision benchtop electronics and cable connection the detector was able to monitor the gamma rays emitted by ^{18}F radiotracer at 140 MBq flowing in the plastic tubing mimicking the vessels of the phantom .

3. Conclusion

In this study, we employed wearable thin film detector based on 2D perovskite for the online monitoring of the radiation emitted by a radioactive drug used in nuclear medicine, namely ^{18}F radionuclide. The thin film architecture enables easy and low temperature fabrication from solution onto flexible substrate, i.e., the development lightweight wearable patches, highly comfortable if worn from a patient during radiotherapy/diagnostic injection session. Thanks to the low dark current achievable by the detector, based on 2-terminal planar photoconductor pixels with micro-crystalline 2D layered $n = 1$ perovskite PEA_2PbBr_4 active layer, it showed a steep and reproducible photocurrent response under 511 keV gamma rays emitted by the radioactive drug, with signal amplitude scaling with the source activity in the range 95–365 MBq. As a further assessment of its reliability, by exposing the device biased at 5 V to more than 4 h of continuous irradiation, we were able to follow the natural radioactive decay of fluorine and to enstimate the ^{18}F half-life with maximum accuracy deviation within 8%. Finally, the detector has been validated for in situ online monitoring of extravasation event, demonstrating the ability to inspect in real-time all the phases of the process: injection; extravasation; flow out; flushing. A wireless wearable system with a customized electronics was also developed and tested to provide the final proof of concept for real-time and online detection of radiotracer emissions.

4. Experimental Section

Preparation of Radioactive Drug: The radioactive solution used for the present work contains ^{18}F radionuclide produced at IRCCS Reggio Emilia by a medical cyclotron (MINItrace, GE HealthCare, Milwaukee, USA) that accelerates H- at a fixed-energy of 9.6 MeV. The MINItrace ^{18}F target system is designed for production of ^{18}F via the $^{18}O(p,n)^{18}F$ reaction. The nucleophilic ^{18}F is achieved as fluoride ion in aqueous solution and removed from the target by pressure. The radioactivity in the solution is measured with a gas filled ionization chamber dose calibrator (ISOMED 2000, Nuclear System, NUVIA Instruments GmbH, Dresden, Germany). The solution can be contained in syringes or in vials and the instrumentation is properly calibrated.

Perovskite Material Synthesis: To prepare the 2D perovskite solution, the two precursor $C_6H_5C_2H_4NH_3Br$ (PEABr, Sigma-Aldrich >98%) and $PbBr_2$ (Sigma–Aldrich >98%) were mixed in N,N-dimethylformamide (DMF, Sigma–Aldrich 99.8% anhydrous) to prepare a 1 M solution with 2:1 molar ratio. The solution was mixed thoroughly overnight and filtrated through a 0.22 µm PTFE filter prior to use. The precursor powders were weighed in air and the solution was prepared in air.

Detector Fabrication: The pixelated photoconductor was directly fabricated on 125 µm thick PET substrate. During the fabrication process the flexible substrate was attached on a 25 mm x25 mm glass used as carrier. A PDMS solution was prepared by mixing 1:10 w/w of cross-linker to hardener and then diluting it 1:1 w/w with hexane. The solution was then spin-coated at 800 rpm on clean glass carrier, immediately after the clean PET substrate were gently placed on top of the glass/PDMS avoiding bubbles. The substrates were then placed on a hotplate at 150 °C to cross link the PDMS. The Cr/Au interdigitated electrode pattern was fabricated on substrates using direct writing photolithography. The Microposit S1818 positive photoresist was spin coated (4000 rpm for 60 s) and annealed at 110 °C for 1 min. Metallic contacts were patterned by using the ML3 Microwriter (from Durham Magneto Optics). The photoresist was developed

with Microposit MF-319 developer. Then, 10 nm of chromium and 25 nm of gold were deposited by thermal evaporation. Samples were immersed in acetone for 4 h for photoresist lift-off. The channel in the interdigitated pattern was L = 10 µm in length, with a total pixel area of 0.5 mm^2. After the lift-off of the photoresist, the Cr/Au patterns were sonicated in water for 10 min then cleaned in air plasma for 2 min prior to perovskite deposition. The perovskite material was deposited by spin-coating at 2000 rpm for 30 s under a constant flux of nitrogen, followed by an annealing at 120 °C for 15 min in a chamber with constant nitrogen flux. The thickness and roughness of the deposited films have been measured through a Smart WLI—GBS profilometer (Figure S4, Supporting Information). The contact pads are cleaned by gently wiping the area with a DMF soaked cotton swab. The device is then sealed by applying epoxy resin (Dowsil 734 clear) on the edge and placing another PET foil on top.

Irradiation Experimental Setup—PEA_2PbBr_4 Response to ^{18}F: The experiments were carried out at the IRCCS in Reggio Emilia through a 3D-printed frame that hold in place a stepper motor and the sample box. To the motor axis is connected a printed support for the vial in which the radioactive drug is contained. The motor is guided by an Arduino UNO board and an A4988 stepper motor driver. The Arduino is programmed to send a PWM signal to the driver; based on the pulse sequence the driver sends a specific current sequence to the motor coils. The motor moves the source by 180°, in the off state the source is at 15 cm from the sample. In the on state, the source is moved on top of the aluminum window of the metal box. An 8 cm thick lead shield is placed between the source and the sample when the system is in the off state. By moving the gamma source back and forth, is possible to acquire a dynamic response of the detector and the data can be analyzed as in the case of X-ray irradiation. The detector response was measured by a Keithley 6517A electrometer connected to the sample box.

Measuring ^{18}F Decay: A 3D printed support was used to hold a plastic vial filled with radiotracer solution directly above the perovskite detector. The solution was prepared to have an initial activity of 1.8GBq. The four pixels detector was connected to a custom 4-channel read-out electronic board which measured the current continuously during the experiment and kept the 5 V bias constant. The board was communicating via Bluetooth with a control PC that recorded all the readings. The sample and the radioactive drugs were left in a closed room away from the operators to reduce the exposure.

Measuring Radiotracer Emission by Wireless Wearable System: The wearable readout system was developed by INFN-TTLAB with the support of BioAge srl. The hardware section is built of three separate circuit boards stacked in an enclosure together with a small Lithium battery. The top circuit board houses the analog section, equipped with a 8 channel charge integrator system based on the ACF2101 (Texas Instruments) charge integrator, followed by a ADS8332 Analog to Digital Converter (ADC, Texas Instruments). It is optimized for pA level current measurement and reaches a resolution of 0.2 pA for a sampling rate of 10 Hz, or 0.02 pA for 1 Hz sampling rate. The middle circuit board contains an Espressif ESP32 microcontroller and its wireless antenna, while the bottom board contains the power conditioning section and the battery controller. The firmware for the ESP32 manages the device, controlling the charge integrator and ADC timing. It reads the digitized values and provides a server from which the client application(s) can read them.

The desktop application is built on top of the Qt6 graphical library. It displays the sensor readings in real time and allows to send commands to the device to adjust the sensor bias and sampling rate.

Supporting Information

Supporting Information is available from the Wiley Online Library or from the author.

Acknowledgements

L.B. acknowledges RELOAD project funded by CARIPLO-CDP grant "Supporto ai giovani talenti italiani nelle competizioni dell'European Research Council". L.P., E.G., F.F. and M.I. acknowledge the Italian Ministry of Health under the program "5perMille, year 2020"—Project Code 5M-2020-23682114—promoted by the AUSL-IRCCS of Reggio Emilia. The authors acknowledge funding from European Community through the POR-FESR 2014–2020 "FORTRESS" project, grant no. I38D18000150009 (PG/2018/629 121) financed by the Emilia-Romagna Region, and BioAge srl (BIOelectronics and Advanced Genomic Engineering) for the development of wearable electronic readout system. The authors would like to acknowledge Sara Cépic for profilometer images at Department of Physics and Astronomy, University of Bologna.

Conflict of Interest

The authors declare no conflict of interest.

Data Availability Statement

The data that support the findings of this study are available from the corresponding author upon reasonable request.

Keywords

2D hybrid perovskites, extravasation, nuclear medicine, radiopharmaceuticals, wearable detectors

Received: August 1, 2024
Published online:

[1] SAMIRA Action Plan - European Commission. https://energy.ec.europa.eu/topics/nuclear-energy/radiological-and-nuclear-technology-health/samira-action-plan.
[2] G. M. Currie, S. Sanchez, *Radiography* **2021**, *27*, 178.
[3] S. Basu, T. C. Kwee, S. Surti, E. A. Akin, D. Yoo, A. Alavi, *Ann. N. Y. Acad. Sci.* **2011**, *1228*, 1.
[4] D. Delacroix, J. P. Guerre, P. Leblanc, C. Hickman, *Rad. Protect. Dosimet.* **2002**, *98*, 1.
[5] S. R. Cherry, M. Dahlbom, in *PET: Physics, Instrumentation, and Scanners*, (Eds: S. R. Cherry, M. Dahlbom, M. E. Phelps), Springer, New York, NY, **2006**, pp. 1–117.
[6] M. Iori, E. Grassi, L. Piergallini, G. Meglioli, A. Botti, G. Sceni, N. Cucurachi, L. Verzellesi, D. Finocchiaro, A. Versari, B. Fraboni, F. Fioroni, *EJNMMI Phys.* **2023**, *10*, 31.
[7] O. Al Musaimi, *Cancers* **2024**, *16*, 1032.
[8] S. Wilson, D. Osborne, M. Long, J. Knowland, D. R. Fisher, *Health Phys.* **2022**, *123*, 343.
[9] P. Tylski, G. Pina-Jomir, C. Bournaud-Salinas, P. Jalade, *EJNMMI Phys* **2021**, *8*, 33.
[10] I. Hirata, A. Mazzotta, P. Makvandi, I. Cesini, C. Brioschi, A. Ferraris, V. Mattoli, *ACS Sens.* **2023**, *8*, 1017.
[11] L. Strigari, R. Marconi, E. Solfaroli-Camillocci, *Sensors* **2023**, *23*, 2599.
[12] K. Sakhatskyi, B. Turedi, G. J. Matt, E. Wu, A. Sakhatska, V. Bartosh, M. N. Lintangpradipto, R. Naphade, I. Shorubalko, O. F. Mohammed, S. Yakunin, O. M. Bakr, M. V. Kovalenko, *Nat. Photon.* **2023**, *17*, 510.
[13] S. Shrestha, R. Fischer, G. J. Matt, P. Feldner, T. Michel, A. Osvet, I. Levchuk, B. Merle, S. Golkar, H. Chen, S. F. Tedde, O. Schmidt, R. Hock, M. Rührig, M. Göken, W. Heiss, G. Anton, C. J. Brabec, *Nat. Photonics* **2017**, *11*, 436.
[14] B. A. H. Huisman, C. Bordoni, A. Ciavatti, M. Sessolo, B. Fraboni, H. J. Bolink, *Adv. Funct. Mater.* **2024**, *34*, 2308844.
[15] L. Basiricò, S. P. Senanayak, A. Ciavatti, M. Abdi-Jalebi, B. Fraboni, H. Sirringhaus, *Adv. Funct. Mater.* **2019**, *29*, 1902346.

[16] G. Kakavelakis, M. Gedda, A. Panagiotopoulos, E. Kymakis, T. D. Anthopoulos, K. Petridis, *Adv. Sci.* **2020**, *7*, 2002098.
[17] L. Basiricò, A. Ciavatti, B. Fraboni, *Adv. Mater. Technol.* **2021**, *6*, 2000475.
[18] S. Demchyshyn, M. Verdi, L. Basiricò, A. Ciavatti, B. Hailegnaw, D. Cavalcoli, M. C. Scharber, N. S. Sariciftci, M. Kaltenbrunner, B. Fraboni, *Adv. Sci.* **2020**, *7*, 2002586.
[19] M. Girolami, F. Matteocci, S. Pettinato, V. Serpente, E. Bolli, B. Paci, A. Generosi, S. Salvatori, A. Di Carlo, D. M. Trucchi, *Nano-Micro Lett.* **2024**, *16*, 182.
[20] M. Verdi, A. Giuri, A. Ciavatti, A. Rizzo, C. Esposito Corcione, L. Basiricò, S. Colella, B. Fraboni, *Adv. Mater. Interfaces* **2023**, *10*, 2300044.
[21] H. Tsai, F. Liu, S. Shrestha, K. Fernando, S. Tretiak, B. Scott, D. T. Vo, J. Strzalka, W. Nie, *Sci. Adv.* **2020**, *6*, eaay0815.
[22] F. Liu, R. Wu, J. Wei, W. Nie, A. D. Mohite, S. Brovelli, L. Manna, H. Li, *ACS Energy Lett.* **2022**, *7*, 1066.
[23] S. Yakunin, D. N. Dirin, Y. Shynkarenko, V. Morad, I. Cherniukh, O. Nazarenko, D. Kreil, T. Nauser, M. V. Kovalenko, *Nat Photon* **2016**, *10*, 585.
[24] H. Tsai, L. Pan, X. Li, J. Yoo, S. Tretiak, X. Ma, L. R. Cao, W. Nie, *Adv. Opt. Mater.* **2023**, *11*, 2300847.
[25] F. Lédée, A. Ciavatti, M. Verdi, L. Basiricò, B. Fraboni, *Adv. Opt. Mater.* **2021**, *10*, 2101145.
[26] W. Peng, J. Yin, K.-T. Ho, O. Ouellette, M. De Bastiani, B. Murali, O. El Tall, C. Shen, X. Miao, J. Pan, E. Alarousu, J.-H. He, B. S. Ooi, O. F. Mohammed, E. Sargent, O. M. Bakr, *Nano Lett.* **2017**, *17*, 4759.
[27] G. F. Knoll, in *Radiation Detection and Measurements*, John Wiley & Sons, Inc., New York, NY, **2011**.
[28] N. US Department of Commerce, NIST XCOM: Photon Cross Sections Database. http://www.nist.gov/pml/data/xcom/index.cfm **2015**.
[29] L. Pan, I. R. Pandey, Z. Liu, J. A. Peters, D. Y. Chung, C. Hansson, B. W. Wessels, A. Miceli, M. G. Kanatzidis, *J. Appl. Phys.* **2023**, *133*, 194502.